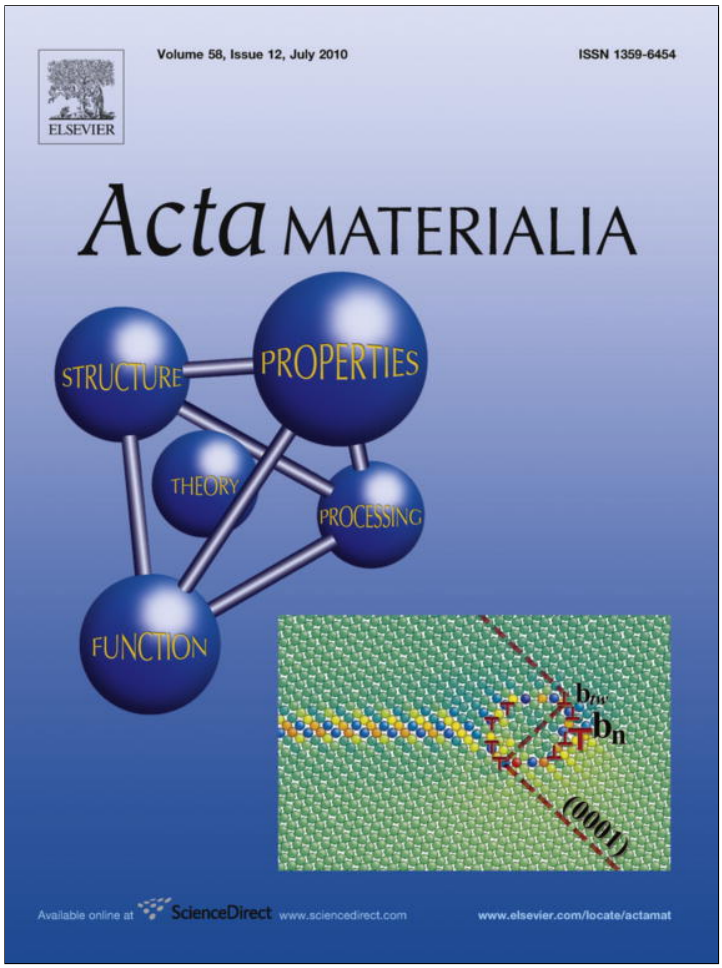

Available online at www.sciencedirect.com
ScienceDirect
Acta Materialia 58 (2010) 4182–4190
Acta MATERIALIA
www.elsevier.com/locate/actamat

Elastic limit for surface step dislocation nucleation in face-centered cubic metals: Temperature and step height dependence

S. Brochard *, P. Hirel [1], L. Pizzagalli, J. Godet

Institut Pprime, CNRS – Université de Poitiers – ENSMA, UPR 3346, Département de Physique et Mécanique des Matériaux, Bvd M. & P. Curie, SP2MI, BP 30179, 86962 Futuroscope Chasseneuil Cedex, France

Received 10 March 2010; received in revised form 2 April 2010; accepted 6 April 2010
Available online 6 May 2010

Abstract

The influences of surface step state and temperature on the elastic limit for dislocation nucleation from a surface step were analyzed by means of atomic scale simulations in face-centered cubic metals. When varying the step height, two regimes were found: for smaller steps, local effects dominate, whereas for larger steps, the stress concentration prevails. The differences observed for the elastic limit were correlated to relevant properties of the different potentials. Finally, for aluminum, the implication of the activation parameters in the nucleation strain was studied in greater detail. This study is particularly relevant to nanostructures, where plasticity is most often governed by dislocation nucleation rather than dislocation multiplication.

Keywords: Dislocation nucleation; Plastic deformation; MD simulations; Surface; Thermally activated processes

1. Introduction

Plasticity in bulk crystals, especially in metals, is most often governed by the multiplication of dislocations from sources, such as Franck–Read sources, and their subsequent glide. However, in nanostructures (thin films, whiskers, nanograined materials, etc.), because of the small dimensions and the low initial density of dislocations, there are no or few active sources to initiate plasticity. Nucleation of dislocations, rather than their multiplication, then becomes a mechanism of prime importance. This feature also appears in the case of nanoindentation, for which dislocation nucleation is commonly associated with the discrete displacements bursts observed in the load–displacement curve, the so-called pop-ins [1–5]. The process of dislocation nucleation has recently regained attention with the development of nanowire/nanopillar deformation tests [5–10]. The mechanical properties of these nanostructures have indeed attracted much interest, not only because they are potential components for the next generation of electronic devices, but also because they are model materials for the study of the elementary mechanisms of plasticity, in particular those related to the size-scale effects usually observed when going towards smaller dimensions [5,6,9–12].

Nanowires and other nanomaterials are characterized by a high surface to volume ratio, so that surfaces are expected to play a key role in dislocation nucleation. In fact, the occurrence of surface dislocation nucleation is supported by experimental evidence [13], in particular in epitaxially strained layers [14–19], though also in the case of indentation [20,21]. From a fundamental standpoint, the mechanism of surface dislocation nucleation is characterized by activation parameters, which define the energy barrier that the dislocation must overcome to be nucleated into the crystal [22,23]. These parameters are intrinsic to the mechanism of dislocation nucleation.

Conversely, "external" parameters, such as the initial surface state, the temperature or the strain rate, can modify the mechanism under consideration, for example by changing

* Corresponding author.
E-mail address: sandrine.brochard@univ-poitiers.fr (S. Brochard).
[1] Present address: Fraunhofer Institut für Werkstoffmechanik, Wöhlerstraße 11, 79108 Freiburg im Breisgau, Germany.

1359-6454/$36.00
doi:10.1016/j.actamat.2010.04.009

the activated glide system [24]. However, their most noticeable expected effect is to modify the elastic limit, here defined as the stress necessary to nucleate the first dislocation. These external parameters are more or less directly controllable experimentally. To gain a deeper insight into the plasticity of nanostructured materials, it is of fundamental importance to determine their role in the dislocation nucleation process.

For example, there are experimental indications that the presence of defects or irregularities on a surface can significantly favor dislocation nucleation [3,14,17,25–27], the main reason invoked being the local stress concentration near the surface defects. The case of a straight surface step on a surface appears to be particularly interesting in this context since it can help dislocation nucleation not only because of the stress concentration but also by the energy gain if the step height is reduced during nucleation. Moreover, being a simple defect, the presence of straight step segments is very likely on real crystal surfaces.

Because of the small space and time scales involved, surface dislocation nucleation events are difficult to observe experimentally, and experiments can hardly provide detailed information on the mechanism, especially where surface steps are concerned. Consequently, several analyses based either on continuum (elasticity) [28–32] or semi-continuum (Peierls–Nabarro) [33,34] models have been developed, all inferring that surface steps are preferential sites for dislocation nucleation. Nevertheless, continuum models do not take into account important atomistic details, and even semi-continuum models, which incorporate a number of atomistic features, rely on assumptions about the mechanism under study (e.g. activated glide systems). Therefore atomic scale simulations seem the best suited for a fine investigation of the nucleation event [22,24,35–40]. In the previous studies using atomic scale simulations, for both face-centered cubic (fcc) metals and covalent silicon, the favorable effect of straight surface steps for dislocation nucleation has clearly been emphasized in two-dimensional [35,36] and three-dimensional [37,38] cases; the conditions required for nucleation to occur have been determined [24,35], the activation parameters have been calculated [22,23,38,39], and in nickel the dislocation nucleation from a surface step has even been examined during growth [40].

Complementarily, the works set out in the present paper aim to study in detail, with atomic scale simulations, the influence of two external parameters on the elastic limit. We consider the case of a surface containing a straight step under stress, and analyze the effect of varying the step height and the temperature. The evolution of the elastic limit with temperature is then correlated with the activation energy. This study is realized on the fcc metals aluminum and copper, because their plasticity is relatively simple and well known (as compared to covalent materials or even body-centered cubic metals). Furthermore, for fcc metals, reliable semi-empirical potentials, based on the embedded atom method (EAM) [41,42], are available. In Section 2, the computational methods used are reported. Then in Section 3, the onset of plasticity is described. The effect of varying the step height is analyzed in Section 4. Finally, the variation of the elastic limit as a function of temperature in the case of monoatomic steps is examined and discussed in relation to activation parameters in Section 5.

2. Methods

2.1. Interatomic potentials

Three different EAM interatomic potentials were used for this study. Most of the calculations were done with the Aslanides and Pontikis (Al–AP) [43] potential for aluminum. We also used the Ercolessi and Adams (Al–EA) [44] potential for aluminum, and the Aslanides and Pontikis (Cu–AP) [43] potential for copper. Some relevant properties of these potentials are listed in Table 1. The same properties for the Mishin et al. potential for copper [45] (used in a comparable study; see Section 5.2) and experimental or ab initio values are also included in Table 1 for comparison. Both potentials for aluminum mainly differ in intrinsic and unstable stacking-fault energies, which are greater and closer to experimental or ab initio values for Al–AP. γ_i and γ_{us} also differ for copper potentials, but the absolute difference between both copper potentials is much smaller than that for aluminum potentials.

2.2. Model geometry

The model system used for this study is a monocrystalline fcc slab with two (1 0 0) free surfaces separated by $10a_0$ (Fig. 1). On one of these surfaces, two steps are built, the step lines being along the [0 1 1] dense direction of the fcc structure. Along this [0 1 1] direction, as well as along the orthogonal [0 $\bar{1}$ 1] direction (also belonging to the surface), periodic boundary conditions are applied, with a length of $15\sqrt{2}a_0$. Thus, our system corresponds to an infinite self-supported thin film with two infinite straight steps on one surface. These steps lie at the intersection between the surface and {1 1 1} planes, so that the geometry is particularly well suited to study glide events in those planes. The system contains 17,700 atoms; though being quite small, the system size is expected to have no influence on the results concerning the very first stages of the nucleation process, which in essence are limited to a small volume. Tests on larger systems (up to 142,800 atoms) have also been performed, showing no significant change in the results in particular in terms of nucleated dislocations and elastic limit.

The slab is then submitted to a uniaxial stress along the [0 $\bar{1}$ 1] direction; that is, orthogonal to the step lines. For this stress orientation, the Schmid factor is maximum in {1 1 1} planes on a Shockley partial dislocation with a Burgers vector orthogonal to the step line (with an edge character if the dislocation line is straight). The stress is applied through the strain calculated using linear elasticity: the system is elongated with a strain ε along [0 $\bar{1}$ 1] and compressed

Table 1
Lattice parameter a_0 at 0 K, thermal expansion coefficient at room temperature α, elastic constants C_{11}, C_{12} and C_{44} and anisotropy ratio A at 0 K, intrinsic γ_i and unstable γ_{us} [53] stacking-fault energies at 0 K for the three EAM potentials used in this study [43,44], for Mishin et al. potential for copper [45] and comparison with experimental (room temperature) or ab initio (0 K) values.

	Al–AP	Al–EA	Al (exp., ab in itio)	Cu–AP	Cu–Mishin [45]	Cu (exp., ab initio)
a_0 (Å)	4.020	4.032	4.05 [47]	3.615	3.615	3.61 [47]
α (10^{-5} K^{-1})	2.3	1.3	2.4 [48]	1.6	≈1.6	1.6 [51]
C_{11} (GPa)	116.5	117.6	106.8 [49]	172.5	169.9	166.1 [52]
C_{12} (GPa)	60.9	62.3	60.4 [49]	119.0	122.6	119.9 [52]
C_{44} (GPa)	29.7	36.7	28.3 [49]	84.8	76.2	75.6 [52]
A	1.07	1.33	1.22 [49]	3.16	3.22	3.27 [52]
γ_i (mJ/m^2)	155	104 [44]	167 ± 33 [50]	29	44	61 ± 17 [50]
γ_{us} (mJ/m^2)	175	125 [46]	199 ± 25 [50]	174	158	184 ± 26 [50]

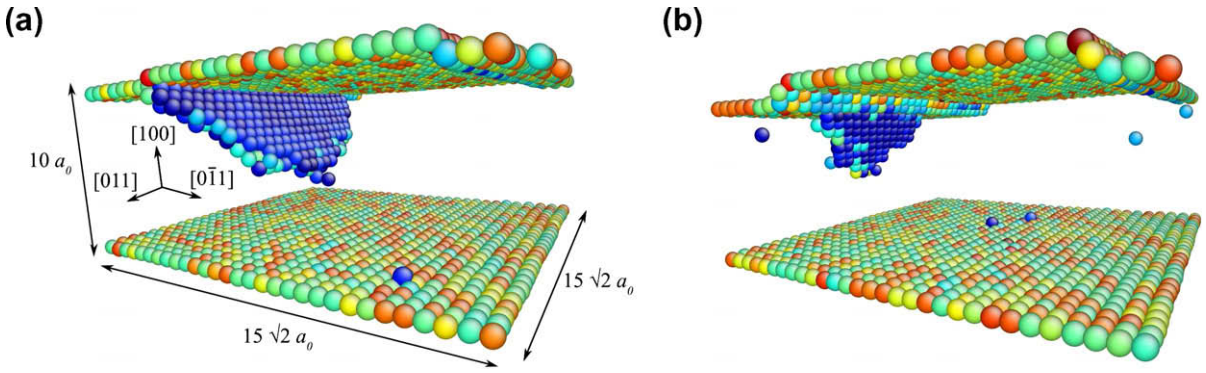

Fig. 1. Typical dislocation half-loop configurations obtained during an MD run at 300 K. (a) Aluminum (AP potential) with initially monoatomic steps under 5.7% applied strain. (b) Aluminum (AP potential) with steps of initial height two atomic layers under 6.2% applied strain. Atoms are colored according to their central symmetry parameter [60]; only atoms which are not in a perfect fcc environment are drawn: surfaces (yellow–green), stacking faults and dislocation cores (blue). (For interpretation of the references to colour in this figure legend, the reader is referred to the web version of this article.)

along [0 1 1] and [1 0 0]. The compression in these two latter directions is simply $v\varepsilon$, v being the Poisson's ratio, for the almost isotropic case of aluminum modeled with the Al–AP potential; for copper and for the Al–EA potential, the compression is calculated using the linear anisotropic elasticity for the specific chosen orientation [54]. The elastic constants used are listed in Table 1. They have been calculated with each potential at 0 K. The elastic constants can vary significantly with temperature. We have checked that using the temperature-dependent elastic constants recently published by Warner and Curtin [46] for the Al–EA potential does not yield differences in the way the strain is applied, which is consistent since the Poisson's ratio was found to be temperature independent by Warner et al. The temperature dependence of the stress–strain relation has not been taken into account here.

2.3. Computational methods

Both 0 K and finite temperature calculations are made. For 0 K calculations, the system is relaxed using a conjugate-gradient algorithm, until the atomic forces are lower than 10^{-3} eV/Å. The strain is increased by 0.1% increments between each energy minimization. Molecular dynamics (MD) simulations at finite temperature are performed at a constant strain rate $\dot{\varepsilon} = 5 \times 10^7$ s^{-1}. This value, typical of MD simulations, is many orders of magnitude larger than experimental ones ($\sim 10^{-3}$ s^{-1}). The strain rate sensitivity of the nucleation stress has been estimated by Zhu et al. [55], who have shown that a reduction in the nucleation stress can amount to up to 50% when passing from strain rate values typical of MD simulations to experimental ones. The time step is no larger than 1 fs, which is small enough to ensure that there is no energy drift for all the temperatures studied. The latter are introduced by giving random initial velocities to all atoms according to the appropriate Maxwell–Boltzmann distribution and maintained by a smooth rescaling of atomic velocities at each MD step.

The thermal expansion is taken into account in this study by using the equilibrium lattice parameter determined for each temperature with the appropriate interatomic potential. Values of the thermal expansion coefficients at room temperature for the three potentials used here are given in Table 1. Not taking into account the thermal expansion, as was done in previous studies [22,37], increases the computed elastic limits for finite temperature calculations, since the system is then slightly compressed and thus the "true" strain is lower than the applied strain. For example, at 300 K the critical strain for nucle-

ation is reduced by 1% (5.6% compared to 6.6%) when the thermal expansion is considered. Obviously, this difference increases with temperature.

The knowledge of the activation parameters, which defines the energy barrier that the system has to cross for a given mechanism to occur, is fundamental in rationalizing the dislocation nucleation event. In this study, the activation energy is determined for different applied strains by means of a static method, the nudged elastic band (NEB) technique [56], specifically designed for the study of transition states. Within the NEB method, the initial and final configurations, independently relaxed, must be provided. A chain of replicas, also called images, is then constructed between the initial and final states. Next, these intermediate images are relaxed, while being constrained by springs, which impede them falling into one of the two minimum energy configurations, i.e. the initial and the final state. The convergence of the whole leads to the minimum energy path (MEP), from which the activation energy, defined as the maximum of the MEP, can be extracted. In this study, we used two refinements of the NEB method: the improved tangent [57] and the climbing image [58].

The initial configuration for the NEB method is constructed here by fully relaxing a deformed system containing no defect, except the monoatomic surface steps. The final configuration consists of a deformed system containing a dislocation half-loop such as obtained during an MD run, with a loop radius just a little bit smaller than the slab thickness. This configuration is relaxed so that its energy is lower than the energy of the initial configuration by several electronvolts. It must be stressed that the final configuration is not fully relaxed, since a full relaxation would yield to the formation of a microtwin [35,37] much too far from the transition state to be used within the NEB method. An alternative way to deal with the final state would be to use the free-end nudged elastic band method [59]. Nevertheless, the fixed final configuration used here is chosen to be far enough from the configuration of the saddle point, and is assumed to be sufficiently relaxed to be close to the MEP. As a result it is sound to assume that it has little influence on the convergence of the MEP near the saddle point or on the activation energy.

Finally, the intermediate images for the NEB method are built using several configurations obtained during an MD run and interpolations. Indeed, the large number of atoms involved in the dislocation nucleation mechanism results in a complex topology in the configuration space, so that a single interpolation between the initial and the final state is not suited for the construction of the intermediate images. MD simulations are a necessary prerequisite here.

3. Description of the onset of plasticity

In the following, the nucleation strain is the applied strain necessary to observe the first plastic event, that is, dislocation(s) nucleation. The elastic limit is defined as the stress corresponding to the nucleation strain calculated using linear anisotropic elasticity with elastic constants given in Table 1. Because of deviation from linearity for high stresses (see e.g. Fig. 2 in Ref. [35] for the Al–AP potential), and since the elastic constants at finite temperature are different from those at 0 K, our calculated elastic limit is not strictly equal to the true stress in the material, even before the occurrence of any plastic event. For example at 300 K, for the Al–EA potential, the elastic limit is overestimated by ~14% when using 0 K elastic constants instead of temperature-dependent ones. Nevertheless, the elastic limit calculated here gives a rough estimate of the stress level present in the material just before dislocation nucleation.

Previous simulations with the Al–AP potential [35,37] have shown that for the chosen stress orientation, and for monoatomic steps, the athermal nucleation strain is ~8.6%, for which two 90° straight Shockley partial dislocations are nucleated from both steps, leaving behind a stacking fault (see e.g. Fig. 2 in Ref. [37]). When temperature is introduced a dislocation half-loop is nucleated for a lower applied strain and from one step [37], as can be seen in Fig. 1. The half-loop is the same kind of Shockley partial as that obtained at 0 K, in agreement with the Schmid factor analysis. For both 0 K and finite temperature calculations, the dislocation is nucleated in the {1 1 1} planes in zone with the step such that the nucleation yields a reduction of the initially monoatomic step height. The appearance of such events is characterized by a sudden drop in the potential energy of the system. In a few cases, we checked that relaxing the stress on these configurations containing the first nucleated dislocation(s) does not produce their disappearance.

The same qualitative results are observed with Al–EA and Cu–AP potentials for monoatomic steps, that is, two

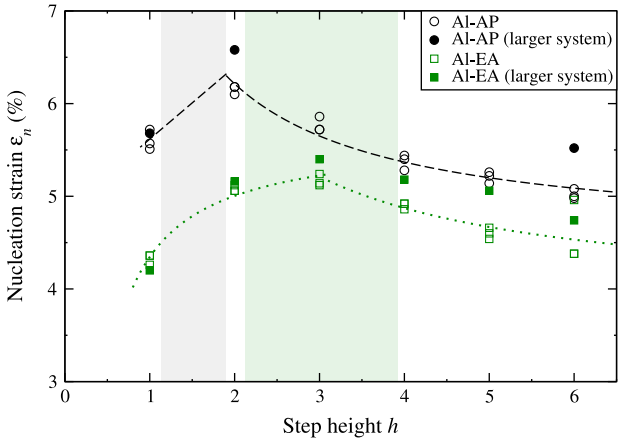

Fig. 2. Nucleation strain obtained at 300 K as a function of the step height h (number of atomic layers) for the Al–AP and Al–EA potentials. The dashed and dotted curves are only guides for eyes. The shaded zones indicate the change of the glide plane activated for the Al–AP (grey, $1 < h < 2$) and Al–EA (green, $2 < h < 4$) potentials, respectively. (For interpretation of the references to colour in this figure legend, the reader is referred to the web version of this article.)

90° straight (0 K) or one half-loop (finite temperature) Shockley partial dislocations are nucleated from the steps, leading to a reduction in the step height. The elastic limits for these events are of course different for the two studied materials, and they also differ between the Al–AP and Al–EA potentials. These differences are described and discussed in Section 5.1.

4. Step height influence

It is sensible to think that changing the step geometry can modify the mechanism of dislocation nucleation and the corresponding nucleation strain, but the particular cases have to be examined with care. For example, in the presence of a few kinks on the steps, unlike what would have been thought at first glance the elastic limit is not modified in comparison with straight steps, but the subsequent motion of the formed dislocation is impeded by the kinks [37]. With a straight step, two beneficial effects are expected for dislocation nucleation: the energy gain associated with a reduction of the step height h and the stress concentration due to the geometrical irregularity on the otherwise plane surface. The latter effect is supposed to grow when the step height increases, whereas the former should barely change. In this section, we analyze the effect of varying the step height on dislocation nucleation at 300 K. The steps are built so as to extend the {1 1 1} planes, yielding a {1 1 1} facet which intersects the (1 0 0) surface along [0 1 1] (Fig. 1b).

The nucleation strains obtained for the Al–AP and Al–EA potentials are shown in Fig. 2 in terms of step height. For step heights larger than two or three atomic layers ($h \geqslant 2-3$), the nucleation strain decreases when the step height increases, which is consistent with the assumption of a greater stress concentration near the step. Using a Peierls–Nabarro approach, confirmed by atomistic calculations in molybdenum and tantalum (0 K and straight dislocations), Li et al. [33,34] obtained a similar effect, though more pronounced than in our case.

What is more amazing is the increase in the nucleation strain observed in Fig. 2 when the step height changes from one to two or three atomic layers. This behavior was obtained for both the Al–AP and Al–EA potentials, suggesting that it is not an artefact of the interatomic potential. This effect seems to contradict the increase in stress concentration as a function of the step height previously invoked. By analyzing the involved mechanisms in greater detail, it can be seen that, for a monoatomic step, the dislocation is always nucleated in the same glide plane, the plane in which the nucleation reduces the step height (Fig. 1a). On the other hand, when the step height is increased, a change in the plane where the dislocation is nucleated is observed (Fig. 1b), the dislocation nucleated always being the same kind of Shockley partial. This change occurs for $h = 2$ atomic layers with the Al–AP potential and for $h = 3$ or 4 atomic layers with the Al–EA potential. Then, after nucleation, the step height is increased. Every time, before nucleation, the von Mises invariant is maximum in the planes where nucleation will occur, revealing that these planes are selected before nucleation.

For a body-centered cubic metal like tantalum, Segall et al. [34] observed a change in the plane in which dislocation nucleation occurs when the step height increases, but did not associate this change with an increase in the critical stress for nucleation. Also, in their calculations the two slip planes where dislocation nucleation occurs were of different families. This implies different crystallographic properties, in particular different generalized stacking-fault energy surfaces. This is not the case here, since both activated glide planes are of {1 1 1} type.

From our results, two regimes were found, the transition between both regimes being characterized by a change in the activated glide plane. For higher steps ($h \gtrsim 2$–3) the stress concentration prevails and the elastic limit decreases when the step height increases. Conversely, for smaller steps the elastic limit unexpectedly increases with the step height. This is probably correlated to a diminution of the stress concentration in the activated glide plane, a plane otherwise favored by some local effects, such as the energy gain due to the reduction of the step height during nucleation. In this latter regime, local effects certainly become predominant.

5. Elastic limit vs. temperature

5.1. Results

In this section, we consider the case of a monoatomic surface step. Fig. 3 shows the variation in the nucleation strain and the corresponding elastic limit as functions of temperature obtained during the MD runs for the three potentials used in this study.

As expected, the elastic limit decreases when temperature increases, whatever the potential. Both potentials for

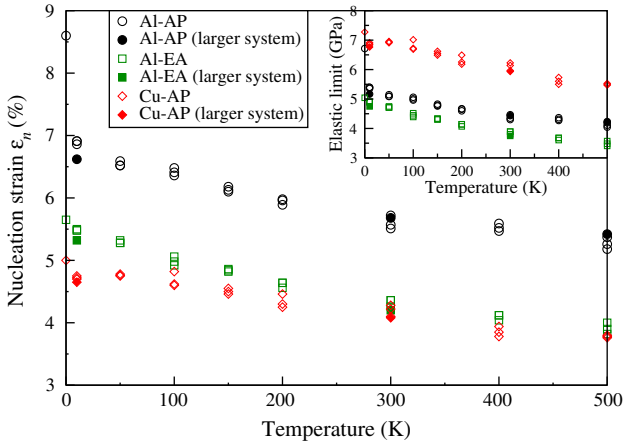

Fig. 3. Evolution of the nucleation strain and the corresponding elastic limit (inset) as functions of temperature obtained during an MD run for the three potentials used in this study.

aluminum show the same variation, with an absolute difference of about 1.4% for the nucleation strain (about 0.6 GPa for the elastic limit), except at 0 K, where the difference amounts to 2.9% for the nucleation strain (1.6 GPa for the elastic limit).

Since for both potentials the ratio $\frac{\gamma_i}{\gamma_{us}}$ and the elastic constants are very close (see Table 1), the differences in the nucleation strain between Al–AP and Al–EA can be ascribed mainly to the difference in the unstable stacking-fault energy γ_{us}, in agreement with the Rice model for dislocation nucleation in a comparable geometry [46,53,61]. As regards the evolution of the nucleation strain between 0 and 10 K, the contrast between both potentials is not so surprising when considering that the mechanism of dislocation nucleation at 0 K differs significantly from that at finite temperature. In the former case the energy barrier for dislocation nucleation must be completely erased by the applied strain, whereas in the latter case the energy barrier is overcome by means of thermal movement, the barrier height varying according to the strain applied. Likewise, the shape of the nucleated dislocation is completely different (straight at 0 K, a half-loop at finite temperature). The way each potential deals with this change in the nucleation mechanism here is markedly distinct, which explains the different evolution in the nucleation strain between 0 K and finite temperature.

For Cu–AP, the unstable stacking-fault energy is of the same order as for Al–AP, but the $\frac{\gamma_i}{\gamma_{us}}$ ratio is smaller; in addition, the elastic constants are globally larger than for aluminum, which implies that for the same strain there is a larger stress in copper than in aluminum. These combined effects yield a lower critical strain in Cu than in Al but a larger elastic limit, as can be seen in Fig. 3.

Constant strain rate and constant stress rate simulations are quite difficult to compare quantitatively because stress and strain are not simply proportional, as mentioned in Section 3. Nonetheless, we compare our results to those obtained with the Mishin et al. potential [45] by Zhu et al. [55] in the case of dislocation nucleation from a copper nanowire corner at constant stress rate (cf. Fig. 3 in Ref. [55]). With a different stress orientation (compression along $\langle 0\,0\,1\rangle$) but the same Schmid factor, Zhu et al. also observed nucleation of a Shockley partial dislocation. The stress levels that they obtained for dislocation nucleation are of the same order but smaller than ours. This could be related to the geometry difference and the resulting stress concentration, and/or to the differences in the intrinsic and unstable stacking-fault energies.

5.2. Discussion

5.2.1. Stochastic model and activation energy

Using a stochastic model, the most probable nucleation strain ε_n can be predicted for a given temperature T if one knows the variation of the activation energy as a function of an applied strain. The implicit equation that has to be solved is [55,62]:

$$\left(\frac{dF_a}{d\varepsilon}\right)_{\varepsilon_n} = -k_B T \frac{v^*}{\dot{\varepsilon}} \exp\left(\frac{-F_a(\varepsilon_n, T)}{k_B T}\right) \quad (1)$$

where $F_a(\varepsilon,T)$ is the activation free energy, v^* is a characteristic frequency (attempt frequency times number of nucleation sites) and $\dot{\varepsilon}$ is the constant strain rate. Hereafter, Eq. (1) is used in the case of dislocation nucleation from a monoatomic surface step, and the calculated most probable nucleation strains are compared to the nucleation strains obtained by direct MD simulations for Al–AP. We want to show in this way that the nucleation strain is very sensitive to small changes in the activation volume.

Following Zhu et al, we consider as a first approximation that the activation free energy can be written as a function of the activation internal energy: $F_a(\varepsilon, T) = \left(1 - \frac{T}{T_m}\right) E_a(\varepsilon)$. In their study, Zhu et al. define T_m as the surface disordering temperature and take it to be equal to half the bulk melting temperature, and they evaluate v^* from NEB calculations. Here, we rather consider T_m and v^* as fitting parameters, since their values are not precisely known and their determination is beyond the scope of this paper.

As mentioned above, the essential input for the use of Eq. (1) is the variation of the activation internal energy as a function of applied strain. By means of an elastic model, the activation internal energy for dislocation nucleation from a surface step has been determined [22,23]. Nevertheless, we pointed out in Ref. [22] some limitations of this elastic model, and indicated that complementary methods, such as the NEB method, have to be used in order to obtain accurate values of the activation energy. Fig. 4 shows the dependence on strain of the activation internal energy $E_a(\varepsilon)$ for half-loop dislocation nucleation from a surface step, obtained with the Al–AP potential using the NEB method, as explained in Section 2. The point determined from MD results with an Arrhenius method and the curve obtained from the elastic model [22,23] are also represented in Fig. 4.

It can be seen in Fig. 4 that the activation energies calculated with the elastic model do not perfectly match those from the NEB method. As suggested by Li [63], the general form $A(1 - \varepsilon/\varepsilon_{ath})^n$ can be used to obtain a better fit to the NEB points. Here $A = 499.6$ eV, $n = 7.02$ and $\varepsilon_{ath} = 8.6\%$. The most probable nucleation strain can then be calculated with Eq. (1), using either the elastic model or the $A(1 - \varepsilon/\varepsilon_{ath})^n$ fit for the activation energy. The latter was first used in order to determine the values of T_m and v^* that best fit the MD nucleation strains. The results, with $T_m = 800$ K and $v^* = 10^{11}$ Hz, are shown in Fig. 5 (dashed curve). These T_m, v^* values seem reasonable when compared to the melting temperature (~930 K) and the Debye frequency (~10^{13} Hz) of aluminum, and the agreement with MD nucleation strains is excellent.

The same T_m and v^* values were used in Eq. (1) with the activation energy now given by the elastic model. As expected, the agreement with the MD nucleation strains is

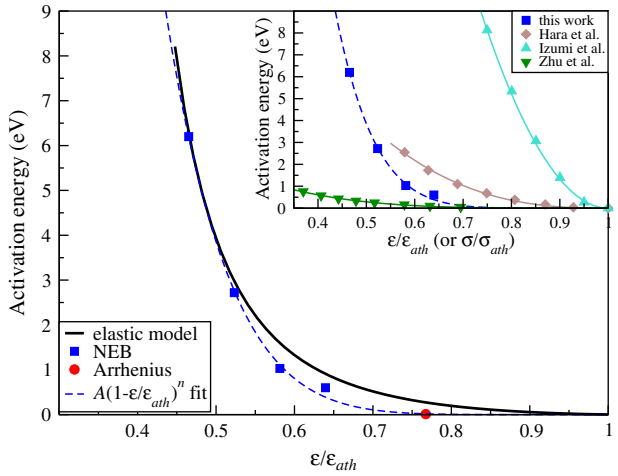

Fig. 4. Dependence of activation energy on applied strain for dislocation nucleation from a surface step. Squares and circle show the values obtained in this study for the Al–AP potential with the NEB method (squares) and the Arrhenius method (circle). The solid line is obtained from an elastic model [22,23] and the dashed line is a fit of the form $A(1-\varepsilon/\varepsilon_{ath})^n$ to the NEB points, where $A = 499.6$ eV, $n = 7.02$ and $\varepsilon_{ath} = 8.6\%$. The inset shows the results determined by Hara et al. [38], Izumi and Yip [39] and Zhu et al. [55], together with the results obtained in this work. All values are plotted as a function of $\varepsilon/\varepsilon_{ath}$, where ε is the applied strain and ε_{ath} the athermal nucleation strain, except those for Zhu et al., which are plotted as a function of σ/σ_{ath}, σ being the applied stress and σ_{ath} the athermal nucleation stress.

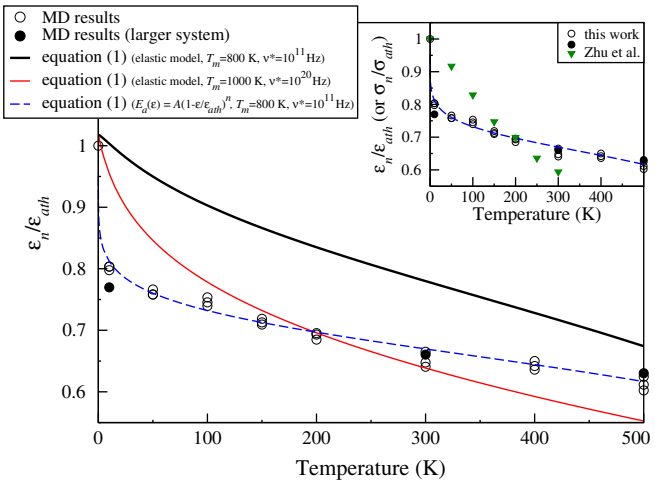

Fig. 5. Dependence of nucleation strain on temperature for dislocation nucleation from a surface step: MD results with Al–AP potential for a small (open circles) and a large (full circles) system (identical to Fig. 3). The dashed line is obtained from Eq. (1) with the dashed curve ($A(1-\varepsilon/\varepsilon_{ath})^n$ form) shown in Fig. 4 for activation energy and $T_m = 800$ K and $\nu^* = 10^{11}$ Hz. The solid lines are obtained from Eq. (1) with the solid curve (elastic model) shown in Fig. 4 for activation energy and $T_m = 800$ K and $\nu^* = 10^{11}$ Hz (thick line) or $T_m = 1000$ K and $\nu^* = 10^{20}$ Hz (thin line). Inset: the triangles show the results obtained by direct MD simulations for the nucleation stress from a nanowire corner by Zhu et al. [55].

not so good (Fig. 5, thick solid line). A better fit can be found by adjusting the T_m and $\nu*$ values, but, as can be seen in Fig. 5 (thin solid line), even with an important latitude for these parameters, leading to unrealistic values, the agreement with MD nucleation strains is far from being correct. Eventually, the strong sensitivity of the nucleation strain to the activation internal energy, and more specifically to the curvature of the $E_a(\varepsilon)$ curve, is evidenced in Fig. 5.

5.2.2. Comparison with previous work: geometrical effect

The activation energies determined for dislocation nucleation from a monoatomic surface step in nickel by Hara et al. [38], from a sharp corner in silicon by Izumi and Yip [39] and from the corner of a copper wire by Zhu et al. [55] are plotted in the inset of Fig. 4 for comparison with our data. Compared to previous studies, the activation energy that we obtain is characterized by a large curvature in the intermediate $\varepsilon/\varepsilon_{ath}$ range ($0.55 \lesssim \varepsilon/\varepsilon_{ath} \lesssim 0.75$), i.e. there is a steep variation in the activation volume in this range. Such a curvature influences the dependence on temperature of the nucleation strain significantly, as shown above when comparing the prediction of Eq. (1) using NEB vs. elastic model for the activation energy.

The important role of the activation energy curvature on the determination of nucleation strains/stresses is further highlighted when comparing the variation of the elastic limit with the temperature obtained for the dislocation nucleation from a monoatomic step in aluminum (present study) to that obtained by Zhu et al. for the dislocation nucleation from a nanowire corner in copper, as shown in the inset of Fig. 5. Indeed, in our case the nucleation strain shows a sharp decrease for small temperatures, followed by a smoother regular decrease for larger temperatures. In contrast, for dislocation nucleation from a nanowire corner, the nucleation stress exhibits a strong regular decrease over the whole range of temperatures studied. These different behaviors can be accounted for by the curvature of the $E_a(\varepsilon)$ curve obtained in this study, which is much larger than that obtained by Zhu et al. (inset of Fig. 4).

Finally, the activation energy curves shown in Fig. 4 stem from studies which differ in the investigated materials and geometries. Three different fcc metals were considered by Hara et al., Zhu et al. and us (respectively nickel, copper and aluminum), so the results cannot be compared directly. Nonetheless, it is seen in the inset of Fig. 4 that the $E_a(\varepsilon)$ curve obtained by Hara et al. is much closer to ours than that obtained by Zhu et al. Hara et al. studied dislocation nucleation from a monoatomic surface step under biaxial strain, i.e. a geometry very similar to that considered in this paper, whereas Zhu et al. studied dislocation nucleation from a nanowire corner. It can thus be concluded that the activation energy for dislocation nucleation is strongly dependent on geometry. This effect is especially visible on the variation of the activation volume (the curvature of the $E_a(\varepsilon)$ curve) with the applied stress/strain.

6. Conclusion

In summary, the effects of two external parameters, the surface step state and the temperature, on dislocation

nucleation from a surface step were studied by means of atomic scale simulations. This investigation was carried out on two fcc metals, aluminum and copper.

When varying the step height, an unexpected result was revealed: an increase in the nucleation strain when the step height was increased for smaller steps. This result is linked to the existence of two distinct regimes: one (smaller steps) where local effects dominate and one (higher steps) where the stress concentration prevails.

When the temperature is increased, the nucleation strain (not surprisingly) decreases. Most of the differences observed between the different potentials have been associated with relevant properties of these potentials; for example, the lower values of nucleation strain obtained for the Al–EA potential than for the Al–AP potential could be correlated to the smaller unstable stacking-fault energy value. Besides, for the Al–AP potential, we specifically analyzed the implication of the activation parameters in the lowering of the nucleation strain when temperature is increased. In fact, knowing the activation energy, the most probable nucleation strain can be determined directly using a stochastic model and compared to MD results. In this paper, we used two different but quite close forms of the activation energy: the first one stemming from an elastic model and the second one fitted to NEB calculations. The important sensitivity of the nucleation strain to the activation energy was thus demonstrated. Finally, by comparing the activation energies and nucleation strains/stresses obtained here and in previous studies, we have shown that the geometry has a substantial effect on the elastic limit.

In conclusion, our results underline that a fine analysis of external parameters is essential for a better understanding of the first stages of plasticity in nanostructures, where the elastic limit is generally associated with a discrete event of dislocation nucleation. For such an event, the elastic limit will depend strongly on the geometry, which is particularly variable in nanostructures.

Acknowledgement

We thank D. Rodney for inciting us to use the stochastic model.

References

[1] Page TF, Oliver WC, McHargue CJ. J Mater Res 1992;7:450.
[2] Gerberich WW, Nelson JC, Lilleodden ET, Anderson P, Wyrobek JT. Acta Mater 1996;44:3585.
[3] Corcoran SG, Colton RJ, Lilleodden ET, Gerberich WW. Phys Rev B 1997;55:R16057.
[4] Tromas C, Gaillard Y, Woirgard J. Philos Mag 2006;86:5595.
[5] Nix WD, Greer JR, Feng G, Lilleodden ET. Thin Solid Films 2007;515:3152.
[6] Volkert CA, Lilleodden ET. Philos Mag 2006;86:5567.
[7] Mook WM, Lund MS, Leighton C, Gerberich WW. Mater Sci Eng A 2008;493:12.
[8] Ho Oh S, Legros M, Kiener D, Dehm G. Nature Mater 2009;8:95.
[9] Gerberich WW, Michler J, Mook WM, Ghisleni R, Östlund F, Stauffer DD, et al. J Mater Res 2009;24:898.
[10] Östlund F, Rzepiejewska-Malyska K, Leifer K, Hale LM, Tang Y, Ballarini R, et al. Adv Funct Mater 2009;19:2439.
[11] Uchic MD, Dimiduk DM, Florando JN, Nix WD. Science 2004;305:986.
[12] Maaß R, Van Petegem S, Ma D, Zimmermann J, Grolimund D, Roters F, et al. Acta Mater 2009;57:5996.
[13] Vanhellemont J, Claeys C, Van Landuyt J. Physica (a) 1995;150:497.
[14] Higgs V, Kightley P, Goodhew PJ, Augustus PD. Appl Phys Lett 1991;59:829.
[15] Cullis AG, Pidduck AJ, Emeny MT. J Cryst Growth 1996;158:15.
[16] Androussi Y, Lefebvre A, Benabbas T, François P, Delamarre C, Laval JY, et al. J Cryst Growth 1996;169:209.
[17] Wu X, Weatherly GC. Philos Mag A 2001;81:1489.
[18] Bolkhovityanov YB, Deryabin AS, Gutakovskii AK, Revenko MA, Sokolov LV. Appl Phys Lett 2004;85:6140.
[19] Pichaud B, Burle N, Texier M, Alfonso C, Gailhanou M, Thibault-Pénisson J, et al. Phys Status Solidi C 2009;6:1827.
[20] Ning XJ, Perez XJ, Pirouz P. Philos Mag A 1995;72:837.
[21] Ning XJ, Huvey N. Philos Mag Lett 1996;74:241.
[22] Hirel P, Godet J, Brochard S, Pizzagalli L, Beauchamp P. Phys Rev B 2008;78:064109.
[23] Hirel P, Godet J, Brochard S, Pizzagalli L, Beauchamp P. Phys Rev B 2010;81:059901.
[24] Godet J, Hirel P, Brochard S, Pizzagalli L. J Appl Phys 2009;105:026104.
[25] Tersoff J, LeGoues FK. Phys Rev Lett 1994;72:3570.
[26] Kiely JD, Hwang RQ, Houston JE. Phys Rev Lett 1998;81:4424.
[27] Navarro V, Rodrìguez de la Fuente O, Mascaraque A, Rojo JM. Phys Rev Lett 2008;100:105504.
[28] Jagannadham K, Narayan J. Mater Sci Eng B 1991;8:107.
[29] Jagannadham K, Narayan J. J Electron Mater 1991;20:767.
[30] Beltz GE, Freund LB. Phys Status Solidi (b) 1993;180:303.
[31] Zou J, Cockayne DJH. J Appl Phys 1996;79:7632.
[32] Junqua N, Grilhé J. Philos Mag Lett 1997;75:125.
[33] Li C, Xu G. Philos Mag 2006;86:2957.
[34] Segall DE, Li C, Xu G. Philos Mag 2006;86:5083.
[35] Brochard S, Beauchamp P, Grilhé J. Philos Mag A 2000;80:503.
[36] Godet J, Pizzagalli L, Brochard S, Beauchamp P. Phys Rev B 2004;70:054109.
[37] Hirel P, Brochard S, Pizzagalli L, Beauchamp P. Scripta Mater 2007;57:1141.
[38] Hara S, Izumi S, Sakai S. J Appl Phys 2009;106:093507.
[39] Izumi S, Yip S. J Appl Phys 2008;104:033513.
[40] Liu WC, Shi SQ, Huang H, Woo CH. Comput Mater Sci 2002;23:155.
[41] Daw MS, Baskes M. Phys Rev Lett 1983;50:1285.
[42] Finnis MW, Sinclair JE. Philos Mag A 1984;50:45.
[43] Aslanides A, Pontikis V. Comput Mater Sci 1998;10:401.
[44] Ercolessi F, Adams JB. Europhys Lett 1994;26:583.
[45] Mishin Y, Mehl MJ, Papaconstantopoulos DA, Voter AF, Kress JD. Phys Rev B 2001;63:224106.
[46] Warner DH, Curtin WA. Acta Mater 2009;57:4267.
[47] Kittel C. Introduction to solid state physics. 5th ed. New York: John Wiley & Sons; 1976 [p. 31].
[48] van Lancker M. Metallurgy of Aluminium Alloys. London: Chapman & Hall; 1967 [p. 8].
[49] Thomas JF. Phys Rev 1968;175:955.
[50] Bernstein N, Tadmor EB. Phys Rev B 2004;69:094116.
[51] Okaji M, Yamada N, Kato H, Nara K. Cryogenics 1997;37:251.
[52] Hiki Y, Granato AV. Phys Rev 1966;144:411.
[53] Rice JR. J Mech Phys Solids 1992;40:239.
[54] Hirth JP, Lothe J. Theory of dislocations. 2nd ed. New York: Wiley; 1982 [p. 435].
[55] Zhu T, Li J, Samanta A, Leach A, Gall K. Phys Rev Lett 2008;100:025502.

[56] Jónsson H, Mills G, Jacobsen KW. In: Berne BJ, Ciccoti G, Coker DF, editors. Classical and quantum dynamics in condensed phase simulations. Singapore: World Scientific; 1998. p. 385.
[57] Henkelman G, Jónsson H. J Chem Phys 2000;113:9978.
[58] Henkelman G, Uberuaga BP, Jónsson H. J Chem Phys 2000;113:9901.
[59] Zhu T, Li J, Samanta A, Kim HG, Suresh S. Proc Natl Acad Sci USA 2007;104:3031.
[60] Li J. Modell Simul Mater Sci Eng 2003;11:173.
[61] Rice JR, Beltz GE. J Mech Phys Solids 1994;42:333.
[62] Rodney D. Phys Rev B 2007;76:144108.
[63] Li J. MRS Bull 2007;32:151.